

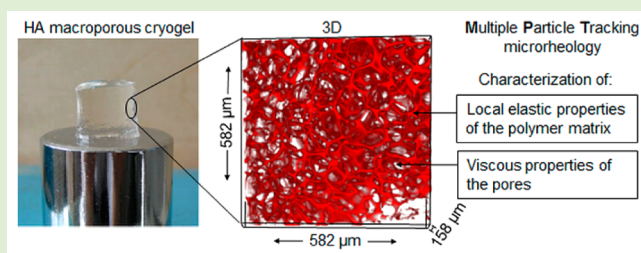
Synthesis, Structural and Micromechanical Properties of 3D Hyaluronic Acid-Based Cryogel Scaffolds

C. Oelschlaeger,* F. Bossler, and N. Willenbacher

Karlsruhe Institute of Technology (KIT), Institute for Mechanical Process Engineering and Mechanics, 76131 Karlsruhe, Germany

S Supporting Information

ABSTRACT: In this study, macroporous, elastic, three-dimensional scaffolds formed of hyaluronic acid mixed with ethylene glycol diglycidyl ether as a chemical cross-linker have been prepared by cryogelation for application in tissue engineering. These cryogels are characterized by large interconnected pores of size $\sim 50\text{--}300\ \mu\text{m}$ and pore wall thickness of $\sim 5\text{--}30\ \mu\text{m}$ as determined from confocal microscopy images. Variation of pH, freezing temperature, and polymerization time allows for control of pore size and shape as well as matrix thickness. These structural properties then determine mechanical strength as well as swelling capacity. Furthermore, increasing hyaluronic acid concentration decreases cryogel pore size, reduces swelling properties, and reinforces mechanical properties. On the other hand, decreasing cross-linker concentration, at a constant hyaluronic acid concentration, increases pore size and swelling capacity but provides less rigidity. Additionally, for the first time, local elastic properties of the polymer matrix and viscous properties of the pores have been characterized using multiple particle tracking microrheology. Local matrix elasticity, relaxation time of hyaluronic acid chains, and the degree of heterogeneity are discussed in detail. These latter properties are crucial for the development of new tissue engineering constructs and will help to understand how local matrix viscoelasticity affects cell cultivation. Finally, elastic moduli obtained in bulk rheology are much higher than corresponding values deduced from microrheology. This discrepancy might be explained by the formation of very highly cross-linked cores in the network where no tracer particle can penetrate.



1. INTRODUCTION

Hyaluronic acid (HA) is a high molecular weight negatively charged polysaccharide composed of repeating disaccharide units of *N*-acetyl glucosamine and glucuronic acid linked by β -1,3 and β -1,4 glycosidic bonds. The number of repeat disaccharides can reach 25 000, which corresponds to a molecular mass of 10^7 Da and a chain contour length of $\approx 10\ \mu\text{m}$.¹ HA is present in all vertebrates, where it is mainly produced by fibroblasts and other specialized tissues cells. It is found primarily in the extracellular matrix (ECM), but has also been shown to occur intracellularly.² The biological functions of HA include maintenance of the viscoelasticity of liquid connective tissues such as joint synovial^{3–6} and eye vitreous fluid, control of tissue hydration and water transport, supramolecular assembly of proteoglycans in the ECM, and numerous receptor-mediated roles in cell detachment, mitosis, migration, tumor development and metastasis, and inflammation.^{7–10} Physical and biochemical properties of HA in solution have been investigated intensively, in particular, rheological,^{11–14} conformational,^{15,16} and structural^{17–19} studies have been performed for a long time, and, more recently, for the first time, microrheological studies.^{20–22} HA properties in solution are of high importance to understand the role of HA in tissue regeneration. In the latter case, HA is used in hydrogel form as a scaffold for tissue engineering (TE). TE holds great promise for regeneration and repair of diseased tissues, making the

development of scaffolds a topic of great interest in biomedical research. For successful TE, the scaffold must be biodegradable and biocompatible, with a 3D porous architecture and interpore connections, and should have appropriate mechanical properties to closely mimic mechanical, and in some cases chemical properties of the ECM. The TE concept involves the seeding of regenerative cells within the scaffolds, the latter serving as a mechanical support and a shape-determining material.

Several approaches to the fabrication of one-component HA and/or HA-mixture 3D porous scaffolds have been developed including phase separation,²³ freeze-drying,^{24–28} electrospinning,²⁹ rapid prototyping,³⁰ porogen leaching,³¹ cross-linking reaction using oxidizing agent,³² templating,³³ and super critical fluid technology.³⁴ Most of these latter techniques are complex, require specific equipment, use high temperatures and organic solvents. In this study, we use a more versatile method, namely, the cryogelation technique to produce macroporous HA scaffolds with control of the pore size using ice crystals as templates without organic solvent, any additives, or cytotoxic porogens. Many review articles^{35–39} and studies^{40–46} have been dedicated to cryogel materials and their application for TE. To the best of our knowledge, only a few studies exist using

Received: November 12, 2015

Revised: January 13, 2016

cryogelation to produce scaffolds from HA. Chang et al.⁴⁷ have shown that macroporous elastic cryogels ($\sim 200\ \mu\text{m}$ pore diameter) could be fabricated from a gelatin and HA mixture for application in adipose tissue engineering. Very recently, Ström et al.⁴⁸ have prepared and investigated physical properties of cross-linked HA cryogels ($100\ \mu\text{m}$ pore diameter). In the latter study, HA was chemically cross-linked with ethylene glycol diglycidyl ether (EGDE). One common characteristic of these cryogels is that the structure is formed of interconnected macropores and that they swell by absorbing large amounts of water. Desirable pore size for TE is typically in the $100\text{--}300\ \mu\text{m}$ range. The role of the pores is to provide the necessary architecture for the three-dimensional organization of cells, to allow supply of nutrients and the removal of waste metabolites³⁶ but most importantly large interconnected pores facilitate blood vessel in-growth.⁴⁹ Despite some studies on this topic^{36,50,51} the role of pore size, volume, and degree of interconnectivity on cell growth and proliferation are still poorly understood, and strategies for a targeted design are lacking. Additionally, cryogel mechanical properties play a fundamental role in the stability of the gels but also in cell adhesion, migration, and proliferation. In general, studies concern macromechanical properties including bulk rheological measurements^{52–58} as well as uniaxial compressive tests.^{26,40,47,59,60} These latter provide Young's modulus E characterizing gel elasticity at the macroscopic scale. Different values of the modulus are connected to different applications, from soft tissues $E \sim (0.1\text{--}1\ \text{kPa})$ to hard bones $E \sim (1\text{--}40\ \text{GPa})$. Gel macroelasticity has also been investigated to study its impact on cell adhesion and proliferation.^{24,25,52–54} Nevertheless, these measurements are not considered ideal, as they probe the gel in its entirety, whereas cell development and behavior are significantly influenced by the elasticity of the microenvironment around them.

Some studies exist in the literature where local viscoelastic properties of the matrix have been investigated by means of atomic force microscopy (AFM) and where the relation between cell and matrix elasticity has been pointed out but only applied to nonporous hydrogels.^{51,61–63} In particular, cell adhesion and morphology change with matrix elasticity. Naive mesenchymal stem cells (MSC), which are initially small and round, develop branched, spindle, or polygonal shapes when grown on polyacrylamide (PA) matrices of moduli $0.1\text{--}1\ \text{kPa}$, $8\text{--}17\ \text{kPa}$, and $25\text{--}40\ \text{kPa}$, respectively.⁵¹ To our knowledge, for porous hydrogels, only one attempt has been performed to characterize matrix local properties but without great satisfaction and efficiency. In this study,⁶⁴ AFM has been used to investigate matrix properties of poly(*N*-isopropylacrylamide) (PNIPAAm) hydrogels with pores of no more than $10\ \mu\text{m}$ in size. Unfortunately, AFM analysis was limited to the inspection of pore surface topology, i.e., surface roughness, and did not at all address the matrix elasticity. Nanoindentation is another technique that has been used to test matrix microscale mechanical properties but also only applied to nonporous hydrogels.^{65,66} To our knowledge, up to now, no nanoindentation studies performed on macroporous hydrogels exist. Several limitations are associated with this technique especially for the study of hydrated samples, as it is the case for cryogels investigated in this study. A first limitation is the surface tension of water and the difficulty to identify the point of zero force. A second one is the softness of the material. Cryogels are considered as soft materials with a Young's modulus $E < 1\ \text{MPa}$, whereas nanoindentation techniques are more adapted

for stiff materials with $E > 1\ \text{GPa}$. The study of soft porous hydrated materials poses many additional challenges in the field of indentation, requiring innovative testing and analysis techniques. In that sense, new techniques providing accurate information about local viscoelastic properties of hydrated soft cryogels are of great importance.

In this study, we have prepared cryogels of similar composition to those produced by Ström et al.,⁴⁸ namely, formed of HA mixed with EGDE as a chemical cross-linker using the cryogelation technique.³⁷ The first part of the study is dedicated to the effect of three different parameters that potentially influence the cryogelation preparation and in turn have an impact on swelling, structural, and mechanical properties. These parameters are the pH exposure time, freezing temperature and kinetics of polymerization. These vary between 10, 15, and 24 h, -18 and $-15\ ^\circ\text{C}$, and 3 and 10 days, respectively. The goal is to have a better control of the overall fabrication process in order to develop a strategy for making gels with well-defined structural and mechanical features. Cryogel pore size and matrix thickness are characterized by confocal laser scanning microscopy (CLSM) images, macromechanical properties by bulk rheometry, and uniaxial compressive tests. Additionally, a systematic study on the influence of HA and cross-linker concentration on gel properties is performed. Two series of cryogel are investigated: a first one with a fixed cross-linker concentration and varying HA concentration and a second one with a fixed HA concentration and varying cross-linker concentration. The second part is dedicated to the characterization of local viscoelastic and microstructural properties of those cryogels. For the first time, we study elastic properties of the matrix and the viscous properties of the pores locally using multiple particle tracking (MPT) microrheology. Accurate characterization of HA networks is of high importance, as the local matrix stiffness is supposed to affect cellular adhesion, migration, and proliferation.^{51–53} Microrheological measurements are performed on cryogels before and after swelling in water using fluorescent polystyrene particles of different diameter (0.5 , 0.2 , and $0.1\ \mu\text{m}$) as tracers. Results are systematically compared to those obtained from macro-rheological measurements.

2. MATERIALS AND METHODS

2.1. Preparation of HA/EGDE Cryogels. HA used in this work was donated by Novozymes Biopharma (Bagsvaerd, Denmark) and is sold under the commercial name Hysis (molecular weight $M_w = 1.43 \times 10^6\ \text{g/mol}$). The production method is based on fermentation of the safe bacterial strain *Bacillus subtilis*. The polydispersity is equal to 1.4, the mass of a disaccharide unit is $400\ \text{g/mol}$, the length of a monomer is $1.02\ \text{nm}$, and the contour length is equal to $L_c = 3.6\ \mu\text{m}$. The cross-linker EGDE was purchased from Polysciences, Inc., Warrington, USA (cat#01479) and has a molecular weight of $174.2\ \text{g/mol}$. This chemical is noncytotoxic and appropriate for cell cultivation. In our study, cryogels were prepared using a different procedure from that of Ström et al.⁴⁸ In the latter study, HA was first dissolved in water before adjusting the pH to 13 with NaOH, whereas in our case HA was first dissolved in a 1 wt % NaOH solution in order to obtain a homogeneous pH adjustment in the whole sample and to ensure efficient cross-linking thereafter. This mixture was maintained for several hours at $4\ ^\circ\text{C}$ until complete dissolution ($\text{pH} \geq 13$). After that, the appropriate amount of EGDE was added to this mixture under stirring (5 min), and then the solution was transferred to syringes that were immersed in glycerol solution stored at low temperature ($-18 \pm 0.1\ ^\circ\text{C}$) in a deep freezer or in a silicon oil bath cooled at $-15 \pm 0.1\ ^\circ\text{C}$ using a commercial immersion thermostat up to 10 days. After

freezing, the solution was heated up to room temperature for at least 2 h before performing experiments. The cryogels thus obtained are spongy, elastic with large interconnected pores and swell instantaneously when immersed in water. An example of a 3D image of the structure of this type of cryogel, obtained by confocal laser scanning microscopy, is shown in the [Supporting Information](#). In this study, we define dry gels as the gels formed just after freezing and which have not been hydrated in water. Hydrated gels correspond to the gels immersed in water and become swollen, accordingly.

2.2. Confocal Laser Scanning Microscopy (CLSM). Pore size images have been taken using a Leica TCS SP8 inverted confocal laser scanning microscope combined with a 20x multi-immersion objective (NA of 0.75). Cryogels were first immersed and stained in an aqueous Rhodamine B solution and then washed several times with Milli-Q water in order to get rid of the dye in the pores. In all CLSM images, pores are colored in black and the HA network in red. The light source was a solid-state laser with an excitation wavelength of 552 nm, and the signal emitted at a wavelength interval of 570 to 700 nm was recorded. The formats of the images were $581 \times 581 \mu\text{m}$ or $775 \times 775 \mu\text{m}$ at a resolution of 512×512 or 1024×1024 pixels, respectively. Average values for pore diameter and statistical errors have been estimated by image analyses of 10 and 5 different pores for [Figures 3B and 7](#) and [Figures 2A,B, 4B, and 9A,B](#), respectively.

2.3. Mechanical Compression Testing. Uniaxial compression tests were performed at room temperature using a commercial Texture Analyzer TAXTplus (Stable Micro System, UK) machine with a 5 kg load cell. Prior to performing compression tests, all cryogels were cut in their swollen state into cylinders of approximately 10 mm in height and 10 mm in diameter. Samples were compressed up to 60% strain at a compression speed of 0.3 mm/s. The Young's modulus, E , has been determined as the initial linear slope of the stress–strain curve, where the stress $\sigma = F/A_0$ and the strain $\varepsilon = \Delta L/L_0$ are defined with respect to the initial dimensions of the sample. F is the compressive force applied to cylindrically shaped gels with an initial surface area of $A_0 = \pi r^2$. ΔL is the change in height of the sample, and L_0 is the initial sample height.

2.4. Rotational Rheometry. A rotational rheometer Thermo MARS II equipped with a smooth plate–plate measuring cell (plate diameter $d_{pp} = 35$ mm, and gap of 2 mm and 5 mm for dry and swollen samples, respectively) was used to perform small amplitude oscillatory shear experiments covering the frequency range from 0.1 to 100 $\text{rad}\cdot\text{s}^{-1}$. Strain sweep experiments performed prior to frequency sweeps ensured that the strain amplitude used was sufficiently small to provide a linear material response at all investigated frequencies. For each experiment no preshear of the gel was performed since in preliminary experiments we have observed variations in the results after repeated measurements on the same gel, probably due to a loss of water with time. Preliminary experiments also confirmed that slip is of minor relevance here due to the large gap. For all gels investigated in microrheology, $G' \gg G''$ and G' is independent of frequency. The plateau modulus $G_{0,\text{Bulk}}$ has been determined as the value of the modulus G' at the frequency at which G'' has its local minimum. All bulk rheological experiments have been performed on gels without tracer particles inside, and we have estimated a relative experimental error of 10%. For microrheology measurements, the plateau modulus $G_{0,\text{MPT}}$ has been determined using the relation $G_{0,\text{MPT}} = \frac{2k_B T}{3\pi a \langle \text{MSD} \rangle}$ where a is the particle radius and $\langle \text{MSD} \rangle$ is the average mean square displacement value in the plateau region where $\langle \text{MSD} \rangle$ is independent of time.

2.5. Multiple Particle Tracking Based Optical Microrheology. MPT experiments were performed using an inverted fluorescence microscope (Axio Observer D1, Zeiss), equipped with a Fluor 100x, N.A. 1.3, oil-immersion lens combined with a 1x optovar magnification changer. We tracked the Brownian motion of green fluorescent polystyrene microspheres of 0.10, 0.19, and $0.51 \mu\text{m}$ diameter (Bangs Laboratories) used as tracer particles. For MPT measurements performed in the pores, after fabrication of the cryogel, the latter was immersed in water and swelled. Then, tracer particles have been directly injected into the gel with a syringe, and these latter go directly

into the pores. On the contrary, for performing measurements in the HA matrix, particles have been added at the first step of the sample preparation, i.e., before freezing. Images of these fluorescent beads were recorded onto a personal computer via a sCMOS camera Zyla X (Andor Technology: 21.8 mm diagonal sCMOS Sensor size, 2160×2160 square pixels). Displacements of particle centers were monitored in an $127 \times 127 \mu\text{m}$ field of view, at a rate of 50 frames/s. Movies of the fluctuating microspheres were analyzed by a custom MPT routine incorporated into the software Image Processing System (Visiometrics iPS) and a self-written Matlab program⁶⁷ based on the widely used Crocker and Grier tracking algorithm.⁶⁸ For both experiments, a relative experimental error of 10% was estimated. Additionally, to perform the statistical analysis and characterize the microstructure heterogeneity, we examined the distribution of displacements, known as the Van Hove correlation function,^{69,70} given by

$$G_s(x, \tau) = \frac{1}{N} \left\langle \sum_{i=1}^N \delta[x + x_i(0) - x_i(\tau)] \right\rangle = \frac{N(x, \tau)}{N} \quad (1)$$

where x is the distance of the particle center of mass along the x -coordinate. $N(x, \tau)$ is the number of particles found at positions between x and $(x + dx)$ after lag time τ (in our study $\tau = 1$ s), and N is the total number of particles. If all particles are exposed to similar environment $G_s(x, \tau)$ has a Gaussian form. Deviations from this form reflect the presence of heterogeneities. Such deviations can be characterized by the non-Gaussian parameter α :⁷¹

$$\alpha = \frac{\langle x^4(\tau) \rangle}{3\langle x^2(\tau) \rangle^2} - 1 \quad (2)$$

This quantity is zero for a Gaussian distribution, while deviations from this distributions can result in large α values.

3. RESULTS AND DISCUSSION

3.1. Variation of Cryogel Properties. **3.1.1. Effect of HA Exposure Time in a NaOH Solution: Role of pH.** The first step of the sample preparation is to dissolve HA in a NaOH solution to reach $\text{pH} > 10$ because the added cross-linker EGDE covalently bonds HA hydroxyl groups only under alkaline conditions. We have observed that the time at which HA is exposed to such high pH plays an important role in cryogel final structure and properties. [Figure 1](#) represents stress–strain

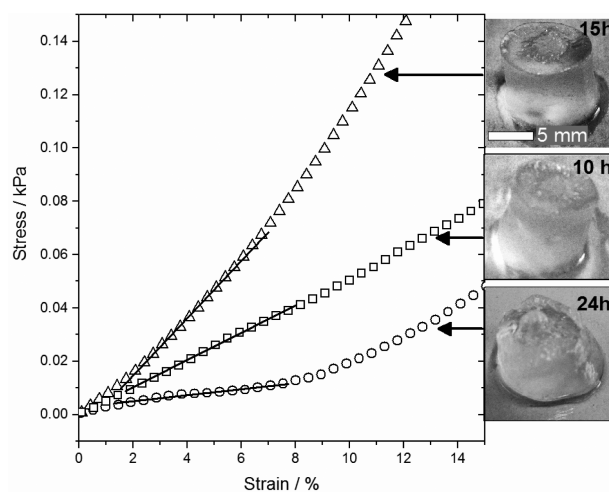


Figure 1. Uniaxial compression tests performed on a HA 3 wt %/EGDE 0.7 wt % cryogel in wet states. Young's modulus E has been determined from the initial linear slope (full line) of the stress–strain curve. Squares, triangles, and circles correspond to 10, 15, 24 h HA dissolution time in a NaOH solution ($\text{pH} > 10$) respectively. Freezing temperature was $-18 \text{ }^\circ\text{C}$, and polymerization time was 3 days.

curves obtained from uniaxial compression tests performed on HA 3 wt %/EGDE 0.7 wt % cryogels prepared with exposure times 10, 15, and 24 h, freezing temperature $-18\text{ }^{\circ}\text{C}$ and polymerization time 3 days. The most stable cryogel is obtained with 15 h exposure time. This gel is highly elastic, with a Young's modulus in the hydrated state (after swelling in water) $E_{\text{hyd}} = 4 \pm 0.8\text{ kPa}$, and stands on its own weight as it is shown in the associated picture. The cryogel with 10 h exposure time is less stable with $E_{\text{hyd}} = 0.55 \pm 0.27\text{ kPa}$ and can hardly stand on its own. This is probably because 10 h is not enough time to allow for a complete HA dissolution and homogeneous dispersion in the solution required for an efficient cross-linking. The weakest cryogel is the one with 24 h exposure time. For the latter, $E_{\text{hyd}} = 0.12 \pm 0.06\text{ kPa}$ and the gel is collapsing under its own weight. The reason presumably is that HA has degraded after 24 h at high pH. It is known that at high pH, HA molecular weight (M_w) degrade due to breakage of H-bonds and cleavage of glucosidic bonds inducing a conformation change of the HA chain from a stiff to a flexible coil.⁷² To summarize, cryogel structure, stability and elasticity depend on the time at which the HA mixture is exposed to high pH. Understanding this point and more generally the role of pH on cryogel properties is of significant importance in order to better control the cryogelation process.

3.1.2. Effect of Freezing Temperature. The second parameter influencing cryogel properties is the freezing temperature. Collins et al.²⁶ have observed that the average pore diameter of HA hydrogels, prepared using the freeze-drying method, decreases from 215 to 156 μm at a freezing temperature of $-20\text{ }^{\circ}\text{C}$ and $-40\text{ }^{\circ}\text{C}$, respectively. In Ström et al.⁴⁸ the pore size decreases from 300 to 150 μm at a freezing temperature of $-10\text{ }^{\circ}\text{C}$ and $-18\text{ }^{\circ}\text{C}$, respectively. With our method of cryogelation, we observe a similar behavior: pores become smaller and wall matrix thinner as the freezing temperature decreases. For the HA 3 wt %/EGDE 0.7 wt % cryogel, pore size decreases from $233 \pm 50\text{ }\mu\text{m}$ to $136 \pm 35\text{ }\mu\text{m}$ and wall thickness from $\sim 100\text{--}40\text{ }\mu\text{m}$ to $\sim 20\text{ }\mu\text{m}$ as the freezing temperature decreases from $-15\text{ }^{\circ}\text{C}$ (Figure 2A) to

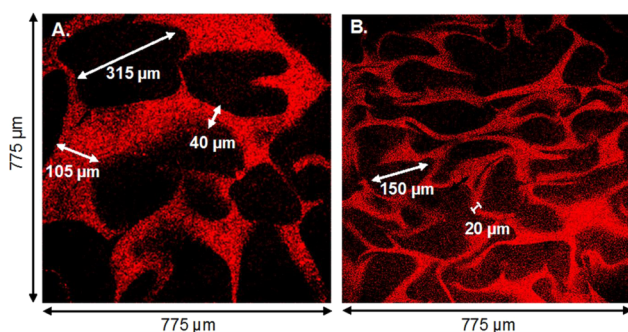


Figure 2. CLSM images of HA 3 wt %/EGDE 0.7 wt % cryogels in the wet state frozen at $-15\text{ }^{\circ}\text{C}$ (A) and $-18\text{ }^{\circ}\text{C}$ (B). In both cases the exposure time in NaOH solution was 15 h and polymerization time 3 days. Cryogels were stained with a rhodamine B solution and rinsed with Milli-Q water afterward to get rid of the dye in the pores.

$-18\text{ }^{\circ}\text{C}$ (Figure 2B) respectively. In both cases, exposure time in NaOH was 15 h, and polymerization time 3 days. At lower temperature, the solvent crystallizes faster, resulting in a large number of small ice crystals acting as pore forming agents. Additionally, we have observed that the pore size is related to the swelling capacity. In fact, the prerequisite for swelling is to

have pore interconnectivity, and the degree of swelling is determined by the degree of cross-linking and polymer concentration. Swelling is less pronounced for samples prepared at lower temperature ($-18\text{ }^{\circ}\text{C}$) where small pores are formed. Swelling ratio $\text{SR} = m_{\text{hyd}}/m_{\text{dry}} = 2$ is found at $-18\text{ }^{\circ}\text{C}$ and $\text{SR} = 5.5$ for preparation at $-15\text{ }^{\circ}\text{C}$. At the same time, the elastic modulus in the hydrated state E_{hyd} is almost constant around $4 \pm 0.8\text{ kPa}$ for both samples.

3.1.3. Effect of Polymerization Kinetics. Finally, we have observed that the kinetics of polymerization also have a significant effect on cryogel structure and properties. Figure 3

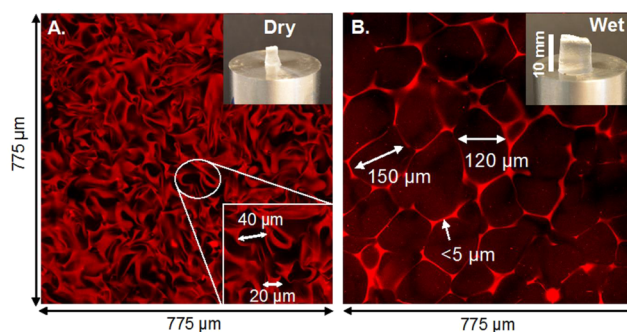


Figure 3. CLSM images of HA 3 wt %/EGDE 0.7 wt % cryogels before (A) and after (B) swelling in a water. (Exposure time in a NaOH solution: 15 h, freezing temperature: $-18\text{ }^{\circ}\text{C}$, and polymerization time: 10 days). Top right in both A and B: photograph of the respective cryogels. Bottom right in A: enlargement of the selected region.

shows the cryogel, after 10 days of polymerization, in the dry (A) and hydrated (B) states before and after swelling in an aqueous solution. This cryogel is a very stable gel with E_{dry} and E_{hyd} equal to $300 \pm 15\text{ kPa}$ and $6.5 \pm 1.3\text{ kPa}$, respectively. The gel structure in the dry state (Figure 3A) shows a very shrunk and dense HA network with small pores of diameter less than 40 μm . The presence of small pores is presumably due to the rest of the Rhodamine–water solution, which is needed to stain the polymer for performing CLSM images. In the hydrated state (Figure 3B), the structure is different compared to the one shown in Figure 2B, where the polymerization time was only 3 days. In both cases, prior to polymerization, the HA storage time at pH = 13 was 15 h, and the freezing temperature was $-18\text{ }^{\circ}\text{C}$. Pore sizes are almost similar ($135 \pm 35\text{ }\mu\text{m}$), but pore shape and matrix thickness differ significantly. For the 10 days polymerization cryogel, pores are more round and homogeneous and the matrix walls much denser and thinner (5 μm or less) compared to 20 μm or more for the 3 days polymerization sample. These structural differences have an important impact on cryogel swelling properties: $\text{SR} = 6$ and 2 were found for gels with 10 and 3 days polymerization time, respectively. At this point, we have clearly shown a significant effect of pH, freezing temperature and polymerization time on the cryogel structure. Pore size and shape as well as matrix thickness change according to the experimental conditions. These structural differences lead to mechanical as well as swelling capacity differences. To summarize, in our study, a macroporous cryogel with appropriate pore size and high mechanical strength is obtained after 15 h exposure time in a NaOH solution, a freezing temperature of $-18\text{ }^{\circ}\text{C}$, and a polymerization time of 10 days.

3.2. Cryogel Local Viscoelastic Properties. 3.2.1. MPT Measurements in the Pores. In multiple particle tracking (MPT) experiments, the thermally driven motion of inert microspheres that are evenly distributed within a fluid is monitored. The resulting particle trajectories are transformed into mean square displacement (MSD) traces. For homogeneous systems, the linear viscoelastic moduli G' and G'' can be extracted from the average MSD. In inhomogeneous systems, the statistical analysis of the MSD distribution provides information about the degree of heterogeneity and the local variation of viscoelastic properties with microscale resolution (0.1–10 μm). Rheological properties are extracted from MSD measurements following the method of Mason et al.⁷³ We have, for the first time, performed MPT measurements on macroporous HA scaffolds. After production of the HA 3 wt %/EGDE 0.7 wt % cryogel (freezing temperature -18°C and polymerization time 3 days), tracer particles of diameter 0.5 μm were directly injected into the gel, and we observed the presence of particles only into the pores and not in the HA matrix as shown in Figure 4A. The latter being probably too

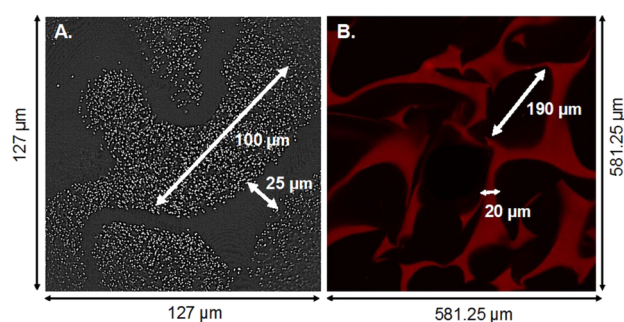


Figure 4. (A) Inverted light microscope image of a HA 3 wt %/EGDE 0.7 wt % cryogel in the wet state. Tracer particles represent PS with a diameter 0.5 μm . (B) CLSM microscope image of the same sample (exposure time in a NaOH solution: 15 h, freezing temperature: -18°C , and polymerization time: 3 days).

highly elastic and strongly cross-linked to allow for penetration of particles into it. In Figure 4A, black areas correspond to the HA matrix with no particles, whereas white areas represent pores containing tracer particles. The pore size is $\sim 100\ \mu\text{m}$ (Figure 4A), and the matrix thickness is $\sim 25\ \mu\text{m}$; these results

are in good agreement with those obtained from CLSM images (Figure 4B) for the same sample. Similar experiments have been performed using gels swollen in aqueous glycerol solutions with 50% and 75% glycerol content. The idea is to modify the viscosity of the solution in the pores. Figure 5 shows the MSD variation of tracer particles with diameter 0.5 μm dispersed only in the pores of the gel swollen in these different solutions. In all cases, the MSD traces vary almost linearly with time, indicating that the motion of the tracer particles is purely diffusive and that the microenvironment surrounding the particles responds like a viscous liquid. From the averaged MSD, we determined the viscosity η_{MPT} using the relation $\langle \Delta r^2(\tau) \rangle = 4D\tau$ where the Stokes–Einstein relation gives $D = \frac{k_B T}{6\pi\eta_{\text{MPT}}a}$ and a is the tracer particle radius. We found $\eta_{\text{MPT}} = 0.9 \pm 0.2, 7.4 \pm 1, 32 \pm 5\ \text{mPa}\cdot\text{s}$ for pure water, 50% and 75% glycerol solutions, respectively. These values are in good agreement with viscosity values of corresponding glycerol/water mixtures determined from bulk rheological measurements: i.e., $\eta_{\text{Bulk}} = 1, 6, \text{ and } 35\ \text{mPa}\cdot\text{s}$, respectively. Additionally, for all solutions investigated above, we have performed statistical analyses of the MSD distribution, and we found low values of α with $\alpha = 0.2, 0.01, 0.02$ for pure water, 50% and 75% glycerol solutions, respectively. This result clearly reveals a homogeneous structure on the micrometer length scale, i.e., that these large pores are uniformly filled with the different fluids and that they do not contain any dissolved non-cross-linked polymer. The slightly higher α value for pure water is due to a very fast diffusion of the particles in and out of the focal plane, leading to some tracking errors but it still confirms a high degree of homogeneity of the system. In summary, we have shown that MPT measurements allow measurement of the viscosity only in the pores. This information may be very useful for the control of cell and nutrient diffusion in the pores.

3.2.2. MPT Measurements in the HA Matrix of a Dry and Hydrated Gel. Contrary to the previous case, where tracer particles were added after gel formation, here particles have been added at the first step of the sample preparation, i.e., before freezing. In this case, after gel formation, no particles were dispersed inside the pores, but they were all trapped in the HA matrix formed during polymerization. One possible explanation for this phenomenon may be that during the freezing process the ice-crystal growth front pushes particles

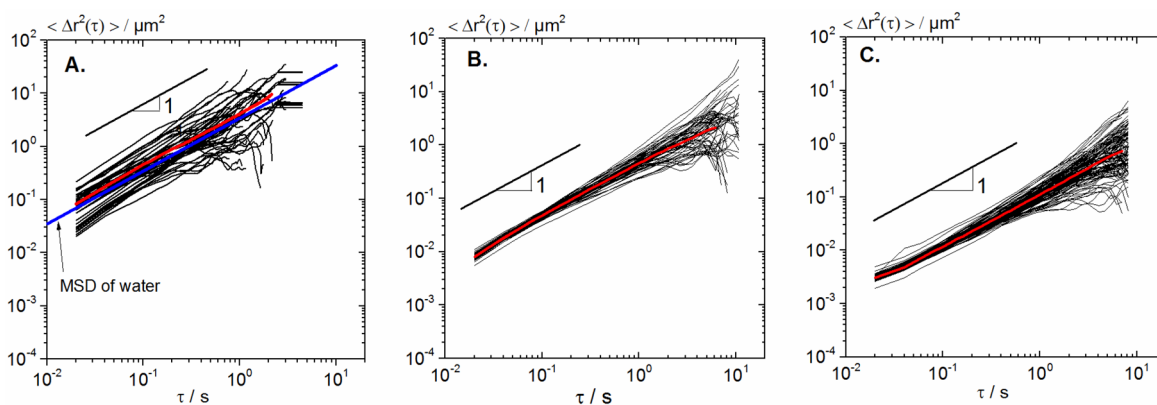


Figure 5. Mean square displacements (MSDs) of individual polystyrene (PS) microspheres of diameter 0.5 μm dispersed in pure water (A), glycerol 50% (B), and glycerol 75% (C) solutions. The red curve is the ensemble-average MSD. The blue curve in (A) represents the theoretical MSD of a 0.5 μm particle dispersed in water with a viscosity of 1 mPa·s at 20°C (exposure time in a NaOH solution: 15 h, freezing temperature: -18°C and polymerization time: 3 days).

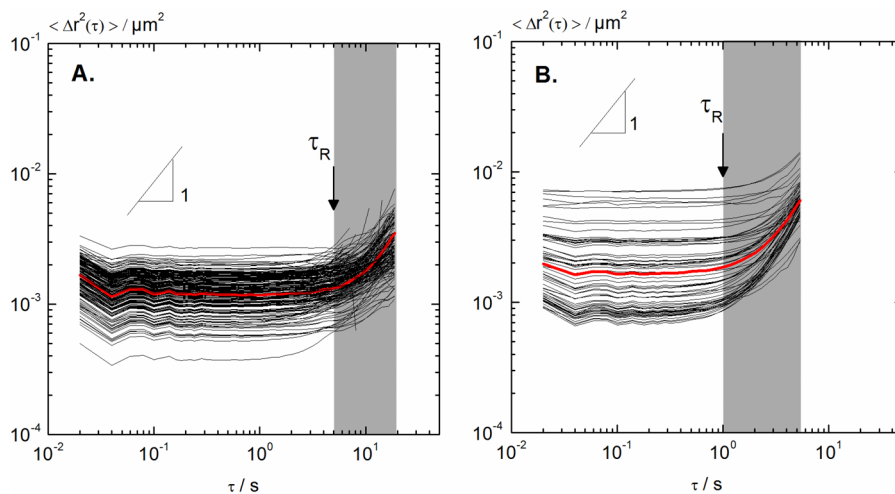


Figure 6. MSDs of PS particles of diameter $0.2 \mu\text{m}$ dispersed in the matrix of a HA 3 wt %/EGDE 0.7 wt % cryogel. (A) Before swelling in the dry state. (B) After swelling in the hydrated state. The red region indicates times $\tau > \tau_R$ (exposure time in a NaOH solution: 15 h, freezing temperature: -18°C and polymerization time: 10 days).

out of the pores. Figure 6 shows the variation of MSDs as a function of time for PS particles of diameter $0.2 \mu\text{m}$ dispersed in the matrix of a HA 3 wt %/EGDE 0.7 wt % cryogel (exposure time in a NaOH solution: 15 h, freezing temperature: -18°C and polymerization time: 10 days) both in the dry (Figure 6A) and hydrated (Figure 6B) state. In both cases, tracer particle motion is significantly different from diffusion in the pores (Figure 5), and all MSDs exhibit almost no time dependence (slope ≈ 0) for times $\tau < \tau_R$ (τ_R being the time that characterizes the onset of the terminal flow regime) with an average MSD (red curve) value $\sim 10^{-3} \mu\text{m}^2$. The so-called static error as described by Savin et al.⁷⁴ is $10^{-4} \mu\text{m}^2$ and can be neglected here. This result indicates that particles are highly constrained by the surrounding fluid, which is consistent with an elastic trapping of tracer particles in a gel-like network. Additionally, for the measurement in the dry state, $\alpha = 0.15$, indicating a homogeneous HA network, whereas in the hydrated state we observe a slight deviation of the measured displacements from a Gaussian distribution with $\alpha = 0.65$. This indicates a slightly higher degree of heterogeneity of the HA matrix after swelling in an aqueous solution but α is still less than one, reflecting a fairly homogeneous system. At long times ($\tau > \tau_R$) the slope of the MSDs traces increases, indicating slow viscous diffusion of the beads corresponding to a transition into the terminal flow regime. MSD increase is stronger and starts earlier for the hydrated cryogel ($\tau_R \sim 1 \text{ s}$) compared to the dry one ($\tau_R \sim 5 \text{ s}$), which indicates a faster relaxation time of HA chains in the matrix after swelling corresponding to an increase of chain mobility.

The absolute value of the time-independent average MSD at $\tau < \tau_R$ is essentially the same in the dry and swollen state corresponding to a plateau modulus $G_{0,\text{MPT}} = \frac{2k_B T}{3\pi a \langle \text{MSD} \rangle} \approx 10 \pm 1 \text{ Pa}$. From this latter value, we can directly determine the mesh size ξ_{MPT} of the HA network according to the classical theory of rubber elasticity with $G_{0,\text{MPT}} = \frac{k_B T}{\xi_{\text{MPT}}^3}$.⁷⁵ We found $\xi_{\text{MPT}} = 75 \pm 8 \text{ nm}$, and this value is much smaller than the diameter of the embedded tracer particles ($\sim 200 \text{ nm}$) used for MPT measurements and therefore characterizes the elastic properties and network structure in the vicinity of the corresponding tracer particles. This value of $G_{0,\text{MPT}} \approx 10 \text{ Pa}$ is much lower

than that obtained from bulk rheology measurements, $G_{0,\text{Bulk}} \approx 1000 \pm 100 \text{ Pa}$ (results shown in the Supporting Information). Similar results have been obtained, e.g., for keratin intermediate filament networks, where $G_{0,\text{Bulk}} > G_{0,\text{MPT}}$.⁷⁶ A pronounced contribution of stretched, out of equilibrium chain segments was proposed to cause the large $G_{0,\text{Bulk}}$ values found for intermediate filament-networks, especially at low protein concentration. In our case, the discrepancy between $G_{0,\text{Bulk}}$ and $G_{0,\text{MPT}}$ might be understood by assuming chain alignment and formation of transient cross-links between the chains that would give an additional contribution to the elasticity in the case of bulk rheological measurements. Another explanation may be the formation of very highly cross-linked cores in the network, where no tracer particle can penetrate. Such densely cross-linked regions would then contribute to $G_{0,\text{Bulk}}$ but not to $G_{0,\text{MPT}}$. Further investigations need to be performed to gain a deeper insight and to explain this large difference between macro- and microrheological results. We hypothesize that the local modulus $G_{0,\text{MPT}}$ is the relevant physical quantity determining the cell growth within the porous hydrogel.

3.2.3. HA Concentration Effect. In this section we investigate the effect of increasing HA concentration on pore size, swelling and micro/macro mechanical properties. Figure 7 shows a CLSM image of a HA 7 wt %/EGDE 1.6 wt % cryogel

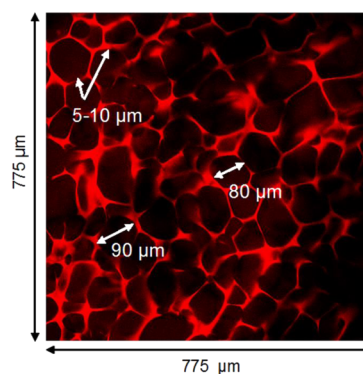


Figure 7. CLSM image of a HA 7 wt %/EGDE 1.6 wt % cryogel after swelling in water. (Exposure time in a NaOH solution: 15 h, freezing temperature: -18°C , and polymerization time: 10 days).

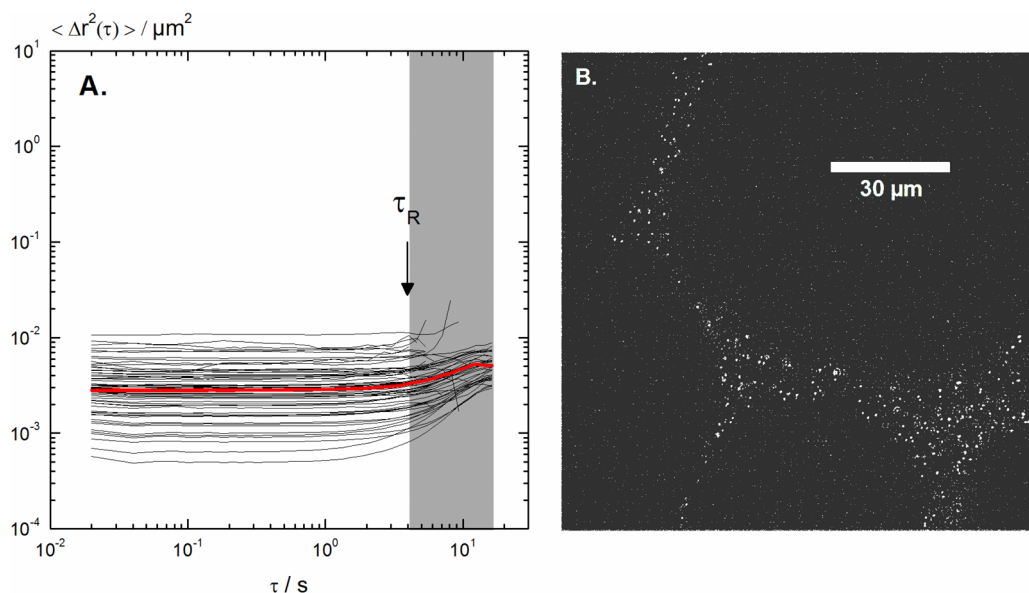


Figure 8. (A) MSDs of PS particles of diameter $0.2 \mu\text{m}$ dispersed in the matrix of a HA 7 wt %/EGDE 1.63 wt % cryogel after swelling in the hydrated state (exposure time in a NaOH solution: 15 h, freezing temperature: $-18 \text{ }^\circ\text{C}$, and polymerization time: 10 days). (B) Corresponding inverted light microscope image.

in the hydrated state with a ratio $R = \text{HA}/\text{EGDE} = 4.3$; this sample was prepared under the same conditions as for the cryogel HA 3 wt % ($R = 4.3$) shown in Figure 3B (exposure time in a NaOH solution: 15 h, freezing temperature: $-18 \text{ }^\circ\text{C}$, and polymerization time: 10 days). We clearly observe a decrease of pore sizes from $135 \pm 35 \mu\text{m}$ to less than $85 \pm 10 \mu\text{m}$ when the HA concentration increases from 3 wt % to 7 wt %, respectively. At the same time the matrix seems to be slightly thicker for the HA 7 wt % ($\sim 5\text{--}10 \mu\text{m}$) compared to the HA 3 wt % ($\leq 5 \mu\text{m}$). This result is presumably due to the fact that for a higher polymer concentration, the initial solution becomes more concentrated. Accordingly, the cross-linking rate will be faster at the same temperature (Kathuria 2009, Lozinsky 2001), leading to gelation in the polymer solution before porogens (ice crystals) are formed. The gel formed under these conditions will have less porosity with smaller pores and thicker pore walls. Additionally, increasing HA concentration leads to reinforced macromechanical properties and reduced swelling capacities. Indeed bulk rheometry measurements show a plateau modulus in the hydrated state $G_{0,\text{Bulk}} = 3000 \pm 300 \text{ Pa}$ and $1000 \pm 100 \text{ Pa}$, and swelling ratios of $\text{SR} = 4.4$ and 6 for HA 7 wt % and HA 3 wt %, respectively. Figure 8A shows the variation of MSDs as a function of time for PS particles of diameter $0.2 \mu\text{m}$ dispersed in the matrix of the HA 7 wt %/EGDE 1.6 wt % cryogel in the hydrated state. Figure 8B shows the corresponding inverted light microscope image. MSDs are almost independent of time over the entire frequency range investigated with $\alpha = 0.7$; this value is similar to that obtained for HA 3 wt % in the hydrated state (Figure 6B), but a slight MSD increase is observed at $\tau_R \sim 4 \text{ s}$ compared to $\tau_R \sim 1 \text{ s}$ for HA 3 wt %. This result indicates a much slower relaxation time of HA chains at higher polymer concentration.

3.2.4. Cross-Linker Concentration Effect. We have also performed measurements on cryogels keeping the HA concentration constant but varying the cross-linker concentration. The goal is to see how the cross-linker concentration affects pore size, swelling, and micro/macro mechanical properties. Figure 9 shows CLSM images of cryogels composed

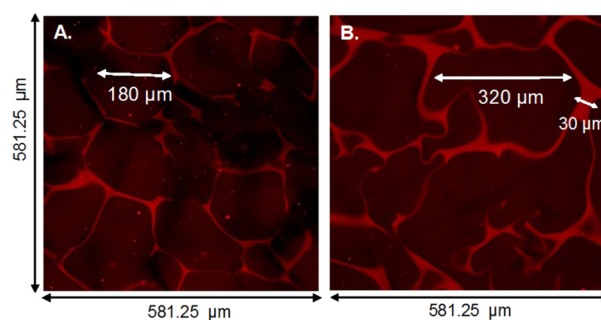


Figure 9. CLSM images of HA 3 wt %/EGDE 0.35 wt % (A) and EGDE 0.15 wt % (B) cryogels after swelling in water (exposure time in a NaOH solution: 15 h, freezing temperature: $-18 \text{ }^\circ\text{C}$, and polymerization time: 10 days).

of HA 3 wt %/EGDE 0.35 (A) and 0.15 wt % (B) in the hydrated state (exposure time in a NaOH solution: 15 h, freezing temperature: $-18 \text{ }^\circ\text{C}$, and polymerization time: 10 days). Comparing these figures with Figure 3B shows that the pore size increases from 135 ± 35 to $260 \pm 86 \mu\text{m}$ and wall matrix thickness from $\leq 5 \mu\text{m}$ to $\sim 30 \mu\text{m}$ when the cross-linker concentration decreases from 0.7 to 0.15 wt %, respectively. Additionally, the cryogel becomes less elastic with the Young's modulus E decreasing from $6.3 \pm 1.26 \text{ kPa}$ to $0.25 \pm 0.13 \text{ kPa}$ and swelling capacity increases from $\text{SR} = 4.9$ to 9.2 . Figures 10A,B shows results of MPT measurements performed in the HA 3 wt % matrix of dry gels with EGDE concentrations 0.7 (A) and 0.15 wt % (B). For the cryogel with lower cross-linker concentration, MSD starts to increase from its initial level at shorter times $\tau_R \approx 2 \text{ s}$, compared to the gel with higher EGDE concentration ($\tau_R \approx 5 \text{ s}$) indicating faster relaxation time of HA chains. This latter result may be related to lower cross-link density and higher swelling capacity in the case of lower cross-linker concentration. Additionally, for the sample with less cross-linker (Figure 10B), the range of displacement at a given lag time is broader than for the one with more cross-linker. At $\tau = 0.1 \text{ s}$, MSD varies more than 1 order of magnitude, from

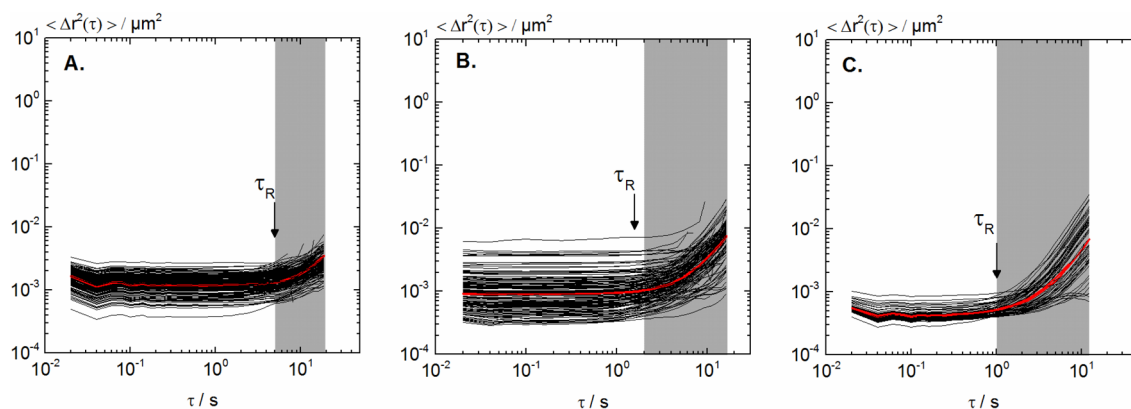


Figure 10. MSDs of PS particles of diameter $0.2 \mu\text{m}$ dispersed in the matrix of a HA 3 wt %/EGDE 0.7 wt % dry state (A), HA 3 wt %/EGDE 0.15 wt % dry state (B), and HA 3 wt %/EGDE 0.15 wt % wet state (C) (exposure time in a NaOH solution: 15 h, freezing temperature: $-18 \text{ }^\circ\text{C}$, and polymerization time: 10 days).

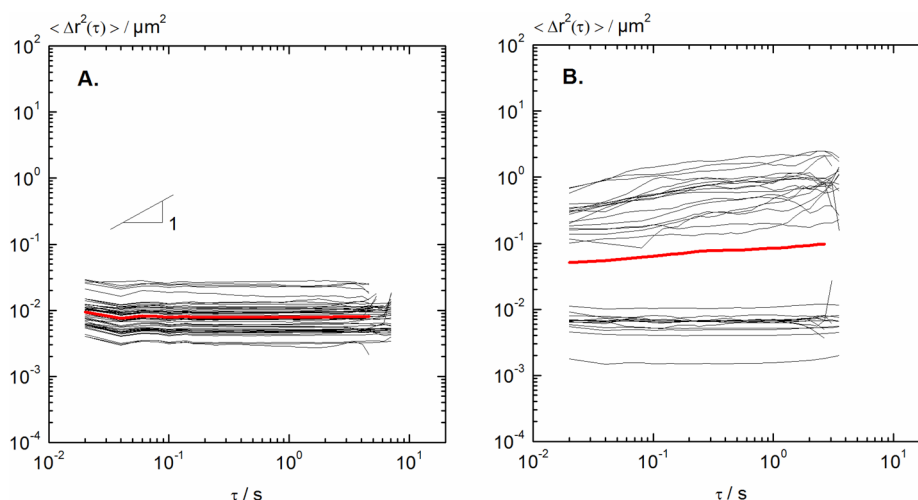


Figure 11. MSDs of PS particles of diameter $0.1 \mu\text{m}$ dispersed in the matrix of a HA 3 wt %/EGDE 0.7 wt % cryogel. (A) In the dry state after 10 days polymerization at $-18 \text{ }^\circ\text{C}$. (B) After 3 days polymerization (exposure time in a NaOH solution: 15 h).

$\sim 3.10^{-4}$ to $5.10^{-3} \mu\text{m}^2$ at lower cross-linker concentration with $\alpha = 0.95$ compared to $\sim 6.10^{-4}$ to $3.10^{-3} \mu\text{m}^2$, at the higher cross-linker concentration and $\alpha = 0.15$. This result indicates a more heterogeneous structure on the micrometer-scale as expected for a presumably incompletely cross-linked network. MPT results obtained for hydrated gels with EGDE 0.7 and 0.15 wt % are shown in Figure 6B and 10C, respectively. The comparison between the dry and wet state for the cryogel with EGDE 0.7% has already been discussed in section 3.2.2. For the cryogel with less cross-linker, a similar observation can be made, that is, the MSD increases earlier in the hydrated state compared to the dry one, but the time difference is much less pronounced with $\tau_R \sim 2 \text{ s}$ and $\tau_R \sim 1 \text{ s}$ in the dry (Figure 10B) and wet (Figure 10C) states, respectively. Another observation is obtained when comparing both gels in the hydrated state (Figure 6B and 10C). In the latter case, contrary to the dry state, the MSD increase occurs at the same time of $\tau_R \sim 1 \text{ s}$. No difference in dynamical properties of the matrix as a function of cross-linker concentration is observed after swelling, whereas it is the case before swelling. Maybe the chains have attained their maximum flexibility and compression after swelling.

3.2.5. Tracer Particle Size Effect. MPT measurements have also been performed in the HA matrix using smaller tracer particles with diameter $0.1 \mu\text{m}$. Figures 11A,B correspond to

measurements in a dry gel after 10 and 3 days polymerization times, respectively. In Figure 11A almost all MSDs traces are time independent with a narrow distribution of absolute values ($\alpha = 0.15$), indicating a homogeneous highly elastic network. On the contrary, for the gel formed during a shorter polymerization time, the MSD distribution is broad and highly asymmetric with $\alpha = 3.65$. Some MSD traces are essentially independent of τ , indicating that the particles are highly constrained by the surrounding solution, and others exhibit a power law time dependence $\text{MSD} \sim \tau$, indicating free diffusion of the particles through the network. This result clearly reveals heterogeneity of this HA network on the length scale of $0.1 \mu\text{m}$. We have shown that the characterization of matrix inhomogeneities is possible by means of MPT measurements. This result is very promising for the investigation of more complex matrices composed for example of mixtures of HA–collagen, HA–chitosan, or HA–protein for which local mechanical heterogeneity may be very important with respect to biological processes, such as cell transport or proliferation.

4. CONCLUSIONS

In this study we have used the cryo-gelation method to fabricate macroporous scaffolds from HA using ethylene glycol diglycidyl ether (EGDE) as a chemical cross-linker. We

obtained deeper insight into the overall fabrication process and develop an efficient strategy for making gels with well-defined structural and mechanical features. In particular, we have shown how various external parameters: pH, freezing temperature, and polymerization time influence cryogel swelling capacity, pore size, and matrix thickness as well as macro-mechanical properties. Additionally, we have shown that increasing HA concentration leads to a decrease of cryogel pore size, reduces swelling properties, and reinforces mechanical properties. On the other side, decreasing cross-linker concentration, at a constant hyaluronic acid concentration, increases pore size and swelling capacities, but provides less rigidity. A very important and promising result of this study is that for the first time local viscoelastic properties of the HA matrix as well as viscous properties of the pores of macroporous cryogels have been characterized using multiple particle tracking (MPT) micro-rheology. In the pores, we have determined the viscosity of diverse solutions, from pure water to water-glycerol mixtures up to 75% glycerol content and have shown in all cases that these solutions are homogeneous. In the matrix, the relaxation time of HA chains of a dry gel is much slower than that obtained after swelling in water corresponding to a higher chain mobility in the hydrated gel. At the same time a slightly higher degree of heterogeneity of the HA network is observed. Additionally, the elastic modulus determined from microrheology is much lower than that obtained from bulk rheometry. For hydrated gels, the relaxation time of HA chains in the matrix becomes slower when increasing HA concentration at constant HA/EGDE ratio, whereas it becomes faster when decreasing the cross-linker concentration at constant HA concentration. Finally, we observe a high degree of inhomogeneity in the matrix on the length scale of 0.1 μm with both elastic and viscous regions for a cryogel made with a three-day polymerization time. In this study we focused on the fabrication and characterization of micromechanical properties of a one-component HA scaffold. These results are very promising for the investigation of more complex matrix for example hybrid scaffold composed of HA and collagen. For the latter system, accurate characterizations of network elasticity and heterogeneity are of high importance, as the collagen content and matrix stiffness affect cell adhesion and growth.

■ ASSOCIATED CONTENT

● Supporting Information

The Supporting Information is available free of charge on the ACS Publications website at DOI: [10.1021/acs.biomac.5b01529](https://doi.org/10.1021/acs.biomac.5b01529).

2D and 3D confocal laser scanning microscopy images of a HA 7 wt %/EGDE 1.63 wt % cryogel, and frequency dependence of bulk shear moduli for a HA 3 wt %/EGDE 0.7 wt % cryogel in the dry state (PDF)

■ AUTHOR INFORMATION

Corresponding Author

*E-mail: claudie.oelschlaeger@kit.edu.

Notes

The authors declare no competing financial interest.

■ ACKNOWLEDGMENTS

The authors thank Kristoffer Tømmeraa (Novozymes A/S, Denmark) for providing the hyaluronan, Laura Lintis and Eva

Hnátková for performing MPT measurements, and Johannes Maurath for compression tests.

■ REFERENCES

- (1) Meyer, K.; Palmer, J. W. *J. Biol. Chem.* **1934**, *107* (3), 629–634.
- (2) Necas, J.; Bartosikova, L.; Brauner, P.; Kolar, J. *Vet. Med.* **2008**, *53* (8), 397–411.
- (3) Neo, H.; Ishimaru, J.-I.; Kurita, K.; Goss, A. N. *J. Oral Maxillofac. Surg.* **1997**, *55* (10), 1114–1119.
- (4) Barbucci, R.; Lamponi, S.; Borzacchiello, A.; Ambrosio, L.; Fini, M.; Torricelli, P.; Giardino, R. *Biomaterials* **2002**, *23* (23), 4503–4513.
- (5) Uthman, I.; Raynauld, J.-P.; Haraoui, B. *Postgrad. Med. J.* **2003**, *79* (934), 449–453.
- (6) Medina, J. M.; Thomas, A.; Denegar, C. R. *J. Fam. Pract.* **2006**, *55* (8), 669–675.
- (7) Balazs, E. A.; Laurent, T. C.; Jeanloz, R. W. *Biochem. J.* **1986**, *235* (3), 903.
- (8) Toole, B. P.; Wight, T. N.; Tammi, M. I. *J. Biol. Chem.* **2002**, *277* (7), 4593–4596.
- (9) Turley, E. A.; Noble, P. W.; Bourguignon, L. Y. W. *J. Biol. Chem.* **2002**, *277* (7), 4589–4592.
- (10) Hascall, V.; Majors, A. K.; De la Motte, C. A.; Evanko, S. P.; Wang, A.; Drazba, J. A.; Strong, S. A.; Wight, T. N. *Biochim. Biophys. Acta, Gen. Subj.* **2004**, *1673* (1–2), 3–12.
- (11) Fouissac, E.; Milas, M.; Rinaudo, M.; Borsali, R. *Macromolecules* **1992**, *25* (21), 5613–5617.
- (12) Fouissac, E.; Milas, M.; Rinaudo, M. *Macromolecules* **1993**, *26*, 6945–6951.
- (13) Rinaudo, M.; Milas, M.; Jouon, N.; Borsali, R. *Polymer* **1993**, *34* (17), 3710–3715.
- (14) Roure, I.; Rinaudo, M.; Milas, M. *Berichte der Bunsengesellschaft/Physical Chem. Chem. Phys.* **1996**, *100* (6), 703–706.
- (15) Cleland, R. L. *Biopolymers* **1984**, *23* (4), 647–666.
- (16) Rinaudo, M.; Roure, I.; Milas, M. *Int. J. Polym. Anal. Charact.* **1999**, *5* (3), 277–287.
- (17) Esquenet, C.; Buhler, E. *Macromolecules* **2002**, *35* (9), 3708–3716.
- (18) Buhler, E.; Boué, F. *Eur. Phys. J. E: Soft Matter Biol. Phys.* **2003**, *10* (2), 89–92.
- (19) Buhler, E.; Boué, F. *Macromolecules* **2004**, *37* (4), 1600–1610.
- (20) Oelschlaeger, C.; Cota Pinto Coelho, M.; Willenbacher, N. *Biomacromolecules* **2013**, *14* (10), 3689–3696.
- (21) Boehm, H.; Munding, T. A.; Boehm, C. H. J.; Hagel, V.; Rauch, U.; Spatz, J. P.; Curtis, J. E. *Soft Matter* **2009**, *5* (21), 4331–4337.
- (22) Nijenhuis, N.; Mizuno, D.; Schmidt, C. F.; Vink, H.; Spaan, J. A. E. *Biomacromolecules* **2008**, *9* (9), 2390–2398.
- (23) Chen, J. Di; Wang, Y.; Chen, X. *J. Biomater. Sci., Polym. Ed.* **2009**, *20* (11), 1555–1565.
- (24) Kim, H. J.; Kim, K. K.; Park, I. K.; Choi, B. S.; Kim, J. H.; Kim, M. S. *Tissue Eng. Regen. Med.* **2012**, *9* (2), 57–62.
- (25) Hwang, H. D.; Cho, H. J.; Balakrishnan, P.; Chung, C. W.; Yoon, I. S.; Oh, Y. K.; Byun, Y.; Kim, D. D. *Colloids Surf., B* **2012**, *91* (1), 106–113.
- (26) Collins, M. N.; Birkinshaw, C. *J. Appl. Polym. Sci.* **2011**, *120* (2), 1040–1049.
- (27) Borzacchiello, A.; Mayol, L.; Ramires, P. a.; Pastorello, A.; Bartolo, C. D.; Ambrosio, L.; Milella, E. *Biomaterials* **2007**, *28* (30), 4399–4408.
- (28) Tian, W. M.; Hou, S. P.; Ma, J.; Zhang, C. L.; Xu, Q. Y.; Lee, I. S.; Li, H. D.; Spector, M.; Cui, F. Z. *Tissue Eng.* **2005**, *11* (3–4), 513–525.
- (29) Nesti, L. J.; Li, W.-J.; Shanti, R. M.; Jiang, Y. J.; Jackson, W.; Freedman, B. A.; Kuklo, T. R.; Giuliani, J. R.; Tuan, R. S. *Tissue Eng., Part A* **2008**, *14* (9), 1527–1537.
- (30) Kang, S.-W.; Kim, J.-S.; Park, K.-S.; Cha, B.-H.; Shim, J.-H.; Kim, J. Y.; Cho, D.-W.; Rhie, J.-W.; Lee, S.-H. *Bone* **2011**, *48* (2), 298–306.
- (31) Flaibani, M.; Elvassore, N. *Mater. Sci. Eng., C* **2012**, *32* (6), 1632–1639.

- (32) Shin, J.; Lee, J. S.; Lee, C.; Park, H.-J.; Yang, K.; Jin, Y.; Ryu, J. H.; Hong, K. S.; Moon, S.-H.; Chung, H.-M.; Yang, H. S.; Um, S. H.; Oh, J.-W.; Kim, D.-I.; Lee, H.; Cho, S.-W. *Adv. Funct. Mater.* **2015**, *25*, 3814–3824.
- (33) Ko, Y.-G.; Oh, H. H.; Kawazoe, N.; Tateishi, T.; Chen, G. J. *Biomater. Sci., Polym. Ed.* **2011**, *22* (1–3), 123–138.
- (34) Barbetta, A.; Carrino, A.; Costantini, M.; Dentini, M. *Soft Matter* **2010**, *6* (20), 5213–5224.
- (35) Fisher, S. A.; Tam, R. Y.; Shoichet, M. S. *Tissue Eng., Part A* **2014**, *20* (5–6), 895–898.
- (36) Henderson, T. M. A.; Ladewig, K.; Haylock, D. N.; McLean, K. M.; O'Connor, A. J. *J. Mater. Chem. B* **2013**, *1* (21), 2682–2695.
- (37) Lozinsky, V. I.; Galaev, I. Y.; Plieva, F. M.; Savina, I. N.; Jungvid, H.; Mattiasson, B. *Trends Biotechnol.* **2003**, *21* (10), 445–451.
- (38) Plieva, F. M.; Galaev, I. Y.; Noppe, W.; Mattiasson, B. *Trends Microbiol.* **2008**, *16* (11), 543–551.
- (39) Carvalho, B. M. A.; Da Silva, S. L.; Da Silva, L. H. M.; Minim, V. P. R.; Da Silva, M. C. H.; Carvalho, L. M.; Minim, L. A. *Sep. Purif. Rev.* **2014**, *43* (3), 241–262.
- (40) Owen, S. C.; Fisher, S. a.; Tam, R. Y.; Nimmo, C. M.; Shoichet, M. S. *Langmuir* **2013**, *29* (24), 7393–7400.
- (41) Kathuria, N.; Tripathi, A.; Kar, K. K.; Kumar, A. *Acta Biomater.* **2009**, *5* (1), 406–418.
- (42) Jain, E.; Srivastava, A.; Kumar, A. *J. Mater. Sci.: Mater. Med.* **2009**, *20* (1), 173–179.
- (43) Reichelt, S.; Becher, J.; Weisser, J.; Prager, A.; Decker, U.; Möller, S.; Berg, A.; Schnabelrauch, M. *Mater. Sci. Eng., C* **2014**, *35* (1), 164–170.
- (44) Plieva, F. M.; Karlsson, M.; Aguilar, M. R.; Gomez, D.; Mikhailovsky, S.; Galaev, I. Y.; Mattiasson, B. *J. Appl. Polym. Sci.* **2006**, *100* (2), 1057–1066.
- (45) Vrana, N. E.; Cahill, P. A.; McGuinness, G. B. *J. Biomed. Mater. Res., Part A* **2010**, *94* (4), 1080–1090.
- (46) Hwang, Y.; Zhang, C.; Varghese, S. J. *Mater. Chem.* **2010**, *20* (2), 345–351.
- (47) Chang, K. H.; Liao, H. T.; Chen, J. P. *Acta Biomater.* **2013**, *9* (11), 9012–9026.
- (48) Ström, A.; Larsson, A.; Okay, O. *J. Appl. Polym. Sci.* **2015**, *132* (29), 42194.
- (49) Kim, B.-S.; Mooney, D. J. *Trends Biotechnol.* **1998**, *16* (5), 224–230.
- (50) Zeltinger, J.; Sherwood, J. K.; Graham, D. A.; Müeller, R.; Griffith, L. G. *Tissue Eng.* **2001**, *7* (5), 557–572.
- (51) Engler, A. J.; Rehfeldt, F.; Sen, S.; Discher, D. E. *Methods Cell Biol.* **2007**, *83*, 521–545.
- (52) Ahearne, M. *Interface Focus* **2014**, *4* (2), 20130038.
- (53) Sharma, A.; Bhat, S.; Nayak, V.; Kumar, A. *Mater. Sci. Eng., C* **2015**, *47*, 298–312.
- (54) Singh, D.; Zo, S. M.; Kumar, A.; Han, S. S. *J. Biomater. Sci., Polym. Ed.* **2013**, *24* (11), 1343–1359.
- (55) Singh, D.; Nayak, V.; Kumar, A. *Int. J. Biol. Sci.* **2010**, *6* (4), 371–381.
- (56) Berillo, D.; Mattiasson, B.; Galaev, I. Y.; Kirsebom, H. *J. Colloid Interface Sci.* **2012**, *368* (1), 226–230.
- (57) Bhat, S.; Kumar, A. *J. Biosci. Bioeng.* **2012**, *114* (6), 663–670.
- (58) Bhat, S.; Tripathi, A.; Kumar, A. *J. R. Soc., Interface* **2011**, *8* (S7), 540–554.
- (59) Loo, S.-L.; Krantz, W. B.; Lim, T.-T.; Fane, A. G.; Hu, X. *Soft Matter* **2013**, *9* (1), 224–234.
- (60) Wang, T. W.; Spector, M. *Acta Biomater.* **2009**, *5* (7), 2371–2384.
- (61) Engler, A. J.; Sen, S.; Sweeney, H. L.; Discher, D. E. *Cell* **2006**, *126* (4), 677–689.
- (62) Engler, A. J.; Richert, L.; Wong, J. Y.; Picart, C.; Discher, D. E. *Surf. Sci.* **2004**, *570* (1–2), 142–154.
- (63) Discher, D. E.; Janmey, P.; Wang, Y.-L. *Science* **2005**, *310* (5751), 1139–1143.
- (64) Zhang, X.; Yang, Y.; Chung, T.; Ma, K. *Langmuir* **2001**, *17* (20), 6094–6099.
- (65) Ebenstein, D. M.; Pruitt, L. a. *J. Biomed. Mater. Res.* **2004**, *69* (2), 222–232.
- (66) Kaufman, J. D.; Miller, G. J.; Morgan, E. F.; Klapperich, C. M. *J. Mater. Res.* **2008**, *23* (05), 1472–1481.
- (67) Kowalczyk, A.; Oelschlaeger, C.; Willenbacher, N. *Polymer* **2015**, *58*, 170–179.
- (68) Crocker, J. C.; Grier, D. G. *J. Colloid Interface Sci.* **1996**, *179* (179), 298–310.
- (69) Hansen, J. P.; Mc Donald, I. . *Theory of Simple Liquids*; Academic Press: London, 1986.
- (70) Van Hove, L. *Phys. Rev.* **1954**, *95* (1), 249–262.
- (71) Weeks, E. R. *Science (Washington, DC, U. S.)* **2000**, *287* (5453), 627–631.
- (72) Gatej, I.; Popa, M.; Rinaudo, M. *Biomacromolecules* **2005**, *6* (1), 61–67.
- (73) Mason, T. G.; Ganesan, K.; Van Zanten, J. H.; Wirtz, D.; Kuo, S. C. *Phys. Rev. Lett.* **1997**, *79* (17), 3282–3285.
- (74) Savin, T.; Doyle, P. S. *Biophys. J.* **2005**, *88* (1), 623–638.
- (75) Rubinstein, M.; Colby, R. *Polymer Physics*; Oxford University Press: Oxford, U.K., 2003.
- (76) Pawelczyk, P.; Mücke, N.; Herrmann, H.; Willenbacher, N. *PLoS One* **2014**, *9* (4), e93194.